RESEARCH PAPER

Peroxide-based route assisted with inverse microemulsion process to well-dispersed $Bi_4Ti_3O_{12}$ nanocrystals

**Jungang Hou · Yuanfang Qu ·
Dalibor Krsmanovic · R. V. Kumar**

Abstract Well-dispersed bismuth titanate (BIT) nanocrystals with an average size ranged from 3 to 60 nm were synthesized via a peroxide-based route assisted with an inverse microemulsion process. The crystallite size and lattice parameter of BIT upon variable-temperature were determined by X-ray diffraction (XRD). The particle size was confirmed by transmission electron microscopy (TEM). Thermal decomposition behaviour of Ti-peroxy and BIT gel and crystallization kinetics of BIT nanocrystals were investigated by differential scanning calorimetry/thermogravimetry (DSC/TG) and Fourier-Transform infrared spectroscopy (FTIR). Analysis of nonisothermal DSC data yielded a value of 220.84 ± 2.73 KJ/mol and 2.25 ± 0.26 for the activation energy of crystallization (E_a) and the Avrami exponent (n), respectively.

Keywords Bismuth titanate · Nanocrystals · Peroxide · Microemulsion · Crystallization

J. Hou · D. Krsmanovic · R. V. Kumar (✉)
Department of Materials Science and Metallurgy,
University of Cambridge, Cambridge CB2 3QZ,
United Kingdom
e-mail: rvk10@cam.ac.uk

J. Hou
e-mail: jh618@cam.ac.uk

J. Hou · Y. Qu
Key Laboratory for Advanced Ceramic and Machining
Technology of Ministry of Education, Tianjin University,
Tianjin 300072, China

Introduction

Ferroelectric materials are potential candidates for high-temperature device applications due to their high dielectric constant, Curie temperature (T_c), breakdown strength and anisotropy and low dielectric dissipation factor, attracting considerable commercial interest in applications such as ferroelectric nonvolatile memories, microelectrome-chanical system, tunable high-frequency devices and integrated photonics (Sugibuchi et al. 1975; Bondurant and Gnadinger 1989; Damjanovic 1998). Bismuth titanate, $Bi_4Ti_3O_{12}$ (BIT), has stimulated intensive attention recently because it is considered to be a potential candidate for lead-free piezoelectric and ferroelectric materials due to their greater environmental acceptability. BIT is a well-known member of the Aurivillius bismuth layer-structured ferroelectrics, which consists of three perovskite-like $(Bi_2Ti_3O_{10})^{2-}$ units with a pseudo-perovskite layer structure, sandwiched between $(Bi_2O_2)^{2+}$ layers (Aurivillius 1949).

Due to considerable interest in BIT, different kinds of methods have been employed to prepare pure and substituted BIT particles and ceramics. Usually, conventional solid-state reaction method have been widely used to prepare BIT ceramics, in which repeated grinding, high sintering temperature and long sintering time were required to achieve high density and homogeneous composition (Kimura et al. 1989). Several alternative chemical synthesis routes

have been proposed such as hydrolysis of metal organic salts (Osamu et al. 1991), coprecipitation method (Horn et al. 1999), sol–gel process (Gu et al. 1998), molten salt synthesis (Kan et al. 2003), templated grain growth (Stojanović et al. 2007), hydrothermal synthesis (Yang et al. 2003), citrate method (Potdar and Ravi 2004), w/o microemulsion route (Xie et al. 2006) and hydrolysis method (Kan et al. 2004). Compared to solid-state reaction method, chemical methods have several advantages, such as low processing temperature, better control of composition, homogeneity, purity and potentially reproducible properties. Despite the excellent properties of these "chemically-prepared" BIT nanocrystals, new problems related to chemical route were found, such as high costs of starting materials or the presence of residual halides when metal chlorides were used. On the other hand, low-temperature chemical process which always needs a large quantity of organics, resulting in the formation of agglomerates has been used to produce the nanoparticles (Hou et al. 2007a, b). Especially, BIT nanoparticles have already been fabricated via a wet-chemical route in our group (Hou et al. 2009a, b). Although they offer a high level of control on the nanoscale but still with a little agglomerates, and the synthesis of well-dispersed perovskite nanocrystals remains a challenge.

A green-chemical technique, originally called the peroxide-based route (PBR), was developed (Camargo and Kakihana 2001). And a water-in-oil microemulsion, which consists of an oil phase, a surfactant and an aqueous phase, is a thermodynamically stable isotropic dispersion of the aqueous phase in the continuous oil phase. Thus, the inverse microemulsion process has some advantages such as much finer in particle size, narrower in particle size distribution and higher in both composition homogeneity and sinterability than other wet-chemical method. Most importantly, bismuth titanate nanocrystals were synthesized at lower temperatures by this new route based on a modified peroxide-based route assisted with an inverse microemulsion process in this report. Metal titanium and hydrogen peroxide was used to prepare nanosized BIT particles. The crystallite size, lattice parameters, particle size of the BIT nanocrystals, crystallization kinetics and morphology were studied using a number of characterization techniques.

Experimental section

BIT nanoparticles preparation

An aqueous solution of hydrogen peroxide (H_2O_2, 99.9%, Aldrich) containing ammonia ($NH_3 \cdot H_2O$, 34 wt%, Aldrich) was prepared. This solution was placed into a cold water bath (at 25 °C) and metal titanium was added. After 5 h, titanium (Ti, 99.5%, Aldrich) was completely dissolved, and a transparent yellow solution containing the soluble peroxytitanato $[Ti(OH)_3O_2]^-$ ion was formed (solution A). An aqueous solution consisting of bismuth nitrate ($Bi(NO_3)_3 \cdot 5H_2O$, 99%, Aldrich) dissolved into nitric acid was obtained (solution B). A microemulsion consisted of butanol (99%, Aldrich), cetyl trimethylammonium bromide (CTAB, 99%, Aldrich) as the surfactant, and *n*-octanol (99%, Aldrich) as the cosurfactant were mixed with solution A and B, and adjusted by a required amount of ammonia solution, then kept for stirring overnight at 60 °C. An orange material was precipitated and isolated by centrifuging (3,000 rpm, 10 min). The orange material was dispersed in a mixture of toluene and hexane, reprecipitated with ethanol, and centrifuged (3,000 rpm, 10 min) to remove the solvent. This dispersing and centrifuging procedure was repeated several times, and then dried in an oven at 100 °C for 2 h. After centrifuging and decanting again, the precipitate was annealed at 450 and 800 °C for 1 h with different heating rate of 10, 15, 20 and 25 °C/min in closed alumina boats. After heat treatment at different annealing temperatures, well-dispersed BIT nanocrystals were obtained under an ultrasonic water bath for 30 min in order to deagglomerate the powder. Flowchart for synthesis of $Bi_4Ti_3O_{12}$ nanocrystals via a peroxide-based route assisted with an inverse microemulsion process was shown in Scheme 1.

Characterization

Phase identification of the as-prepared samples (~2 g) was preformed using XRD through a Scintag diffractometer with Cu K_α radiation, 2θ range between 10° and 110°, step size of 0.02° (2θ), divergence slit = 0.5 mm, receiving slit = 0.3 mm. Parameters used for slit widths and accelerating voltages were identical for all samples. The crystallite sizes were calculated using the Scherrer's formula:
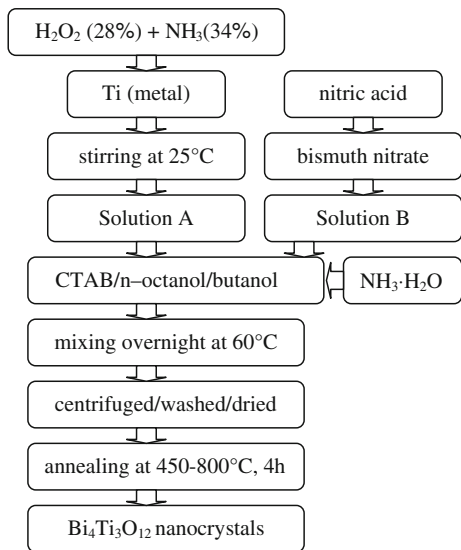
Scheme 1 Flowchart for synthesis of $Bi_4Ti_3O_{12}$ nanocrystals via a peroxide-based route assisted with an inverse microemulsion process

$$B\cos\theta = \frac{0.9\lambda}{D} + 2\frac{\Delta d}{d}\sin\theta \qquad (1)$$

where B represents the full width at half maximum (FWHM) of the peak appearing in the XRD pattern at the angle 2θ, λ is the X-ray wavelength (0.15418 nm), θ the Bragg angle, D is crystallite size in nm, and $\Delta d/d$ the strain. The voltage and current settings of the diffractometer were 40 kV and 40 mA, respectively. The lattice parameters of BIT annealed at various temperatures were calculated using the computer program X'Pert HighScore Plus 2.0. The particle size and morphology analysis was performed by transmission electron microscopy (TEM, Philips CM30). Thermal decomposition behaviour of Ti-peroxy and BIT gel and crystallization kinetics of BIT nanocrystals were investigated separately by DSC-TG (TA Instruments) with various heating rates of 10°, 15°, 20° and 25 °C/min under a continuous air flow (100 mL/min). During the annealing treatment, 10 mg of the precipitate is used for each sample. In order to exploit the difference on the analysis of DSC-TG and FT-IR between BIT gel and Ti-peroxy gel, the sample for Ti-peroxy gel was obtained through dissolving Ti metal into an aqueous solution consisting of hydrogen peroxide and ammonia, and the BIT gel was obtained after drying BIT precursor. FT-IR spectra (Bruker, Tensor 27) were obtained by a

FT-IR spectrophotometer from 350 to 4,000 cm^{-1} by the KBr pellet method.

Results and discussion

Crystallographic analysis

The room-temperature XRD patterns of BIT nanocrystals annealed at different temperatures are shown in Fig. 1. After heat treatment at 450 °C, it has been produced amorphous BIT. It is also found from XRD spectra that the BIT nanocrystals are formed at 550 °C for a duration of 4 h, as observed by XRD using the PBR. In order to exploit more details shown in Fig. 2, BIT samples prepared by this novel route with the annealing temperature of 550 °C for 1, 2 and 4 h, respectively. During this process, the products, $Bi_{20}TiO_{32}$, $Bi_2Ti_2O_7$ and amorphous phase as second phases in $Bi_4Ti_3O_{12}$ nanocrystals as shown in Fig. 2a, appeared at 550 °C for 1 h, and then gradually disappeared with an increase in calcination time up to 4 h. With increasing temperature for a fixed duration of 4 h, the broad hump associated with the amorphous phase decreased, and the intensity of XRD peaks increased while the line width decreased, demonstrating an increase in grain size. The crystallite size of the nanocrystal annealed at 550 °C for 4 h was determined to be approximately 15 nm from the half-width of the X-ray diffraction peaks using Scherrer's equation. The average size calculated was of 15 nm for samples
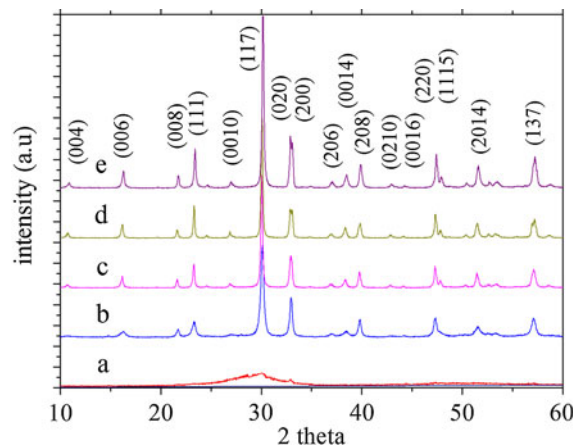
Fig. 1 XRD patterns of BIT nanocrystals annealed at different temperatures: *a* 450 °C, *b* 550 °C, 600 °C, *d* 700 °C and *e* 800 °C °C for a duration of 4 h
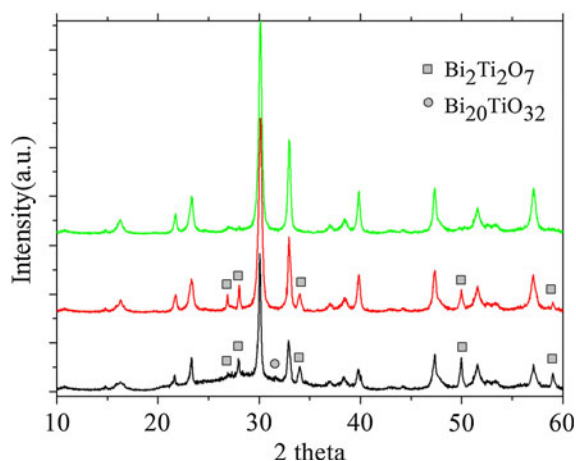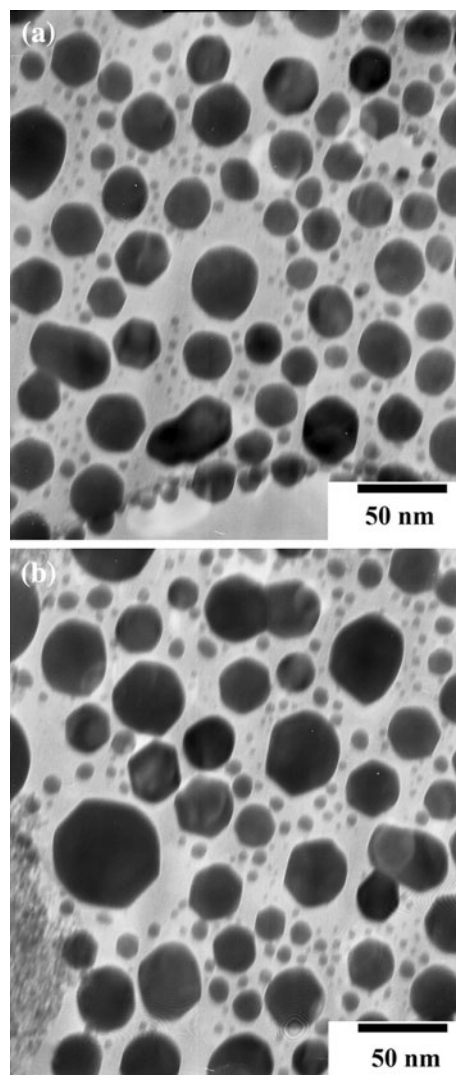
Fig. 2 XRD patterns of BIT nanocrystals annealed at 550 °C for different time: *a* 1 h, *b* 2 h, and *c* 4 h

annealed at 550 °C and 65 nm for samples annealed at 800 °C. The measured lattice parameters of BIT nanocrystals can be calculated as follows. The orthorhombic lattice parameters *a*, *b*, and *c* for the sample annealed at 550 °C were determined to be 5.4496(4), 5.4143(9) and 32.827(2) Å ($R_{wp} = 8.72\%$, $S = 6.43$), which are close to the results for the single crystal (Subbarao 1961), indicating that identical crystal structure has been formed.

Morphology of BIT nanocrystals

Transmission electron microscopy patterns of well-dispersed bismuth titanate nanocrystals annealed at 550 and 600 °C for 4 h are presented in Fig. 3a and b, respectively. The particle size was smaller than 60 nm, with the range of size distribution between 3 and 60 nm, which is consistent with the crystallite size. With increasing annealing temperature, the particle size increased a bit. Histogram of BIT nanocrystals annealed at 550 and 600 °C for 4 h is shown in Fig. 4, demonstrating that the mean diameters of the particles obtained at 550 and 600 °C are 22 and 28 nm with the standard deviation of 5 nm, except for most of small nanocrystals around 3 nm with the standard deviation of 2 nm. Most importantly, the particles prepared by this novel route are well-dispersed. Compared to all abovementioned, such as hydrothermal (Yang et al. 2003), sol–gel process (Gu et al. 1998) and coprecipitation (Horn et al. 1999), as well as metal-organic polymeric precursor process (Hou et al. 2009a, b), the
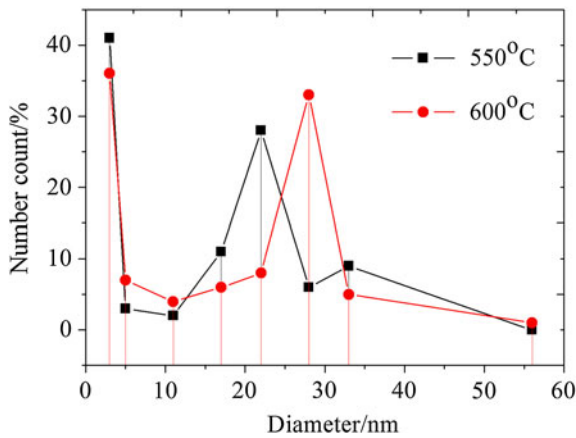

**Fig. 3** TEM patterns of BIT nanocrystals annealed at 550 °C (**a**) and 600 °C (**b**) for 4 h

peroxide-based route assisted with the inverse microemulsion process yields well-dispersed nanocrystals with single phase and small particle size, and has marked advantages over the other chemical synthesis techniques.

Crystallization kinetics analysis

Main characteristics of the precursor can be distinguished in the thermogram shown in Fig. 5. The exothermic peaks in the DSC curve appear below 500 °C which are accompanied by a large weight loss in the TG curves. For the BIT precursor, the weight

Fig. 4 Histogram of BIT nanocrystals annealed at 550 °C *a* and 600 °C *b* for 4 h
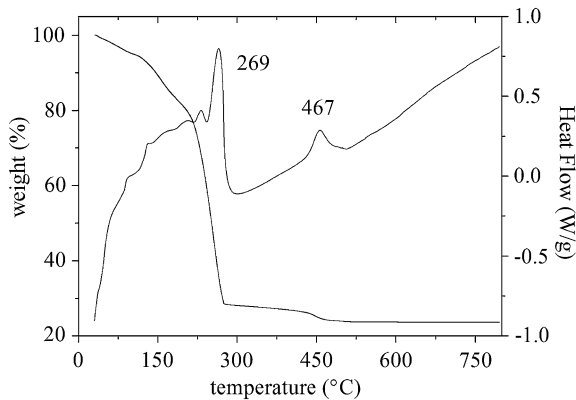
Fig. 5 DSC/TG patterns of BIT precursors, the heating rate was 10 °C/min

loss has taken place in two steps from 25 to 500 °C, with different shape and temperature range (as shown in Fig. 2). First step is from 25 to 300 °C, with 72 wt% weight loss, which is associated with the evaporation of absorbed water and the decomposition of some organics, such as cosurfactant. Second step is seen at approximate 467 °C with the exothermic peak which is ascribed to the crystallization of BIT from the amorphous phase. For temperatures higher than 500 °C, the weight loss is negligible and the weight of BIT nanocrystals appear to be constant.

Crystallization characterization is estimated from the nonisothermal DSC analysis in the BIT nanocrystal. Figure 6 shows the DSC curves of the as-synthesized BIT precursors observed at different heating rates ranging from 10 to 25 °C/min. With

increasing heating rate, the exothermic peak shifted to a higher temperature. The peaks of the crystallization temperature are 467.5, 468.9, 470.7 and 472.6 for the heating rate 10°, 15°, 20° and 25°/min, respectively. The volume fraction of crystallized phase increases with increase of the annealing temperature. These results are consistent with DSC measurement results. The crystallization peaks, depending on the heating rate, can be used to estimate the activation energy for crystallization. The activation energy value for the crystallization can be estimated using the following Kissinger analysis (Kissinger 1956). Through the change in the peak crystallization temperature (T_p) with respect to the heating rate, the activation energy for crystallization could be determined by the Kissinger equation as follows:

$$\mathrm{Ln}\left(T_p^2/\Phi\right) = E/RT_p + cons\tan t \qquad (2)$$

where E is the activation energy for crystallization. T_p is the temperature corresponding to the maximum of the DSC crystallization peak, R is the gas constant (8.314 J/mol), and Φ is the heating rate. From the linear plot of $\mathrm{Ln}(T_p^2/\Phi)$ versus $1/T_p$ the slope is given by E/R, and the activation energy of the crystallization process could be estimated. Figure 7 shows the Kissinger plot of an as-prepared BIT nanocrystal. The activation energy of crystallization is determined by the Kissinger equation to be equal to 95.6 ± 5.6 kJ/mol. Moreover, the Avrami exponent n can be determined from the DSC results. The value of the Avrami parameter n, which is a measure of the dimensionality of transformation, is determined using the Ozawa equation (Ozawa 1971):

$$d\{\mathrm{Ln}[-\mathrm{Ln}(1-x)]\}/d\mathrm{Ln}\Phi = -n \qquad (3)$$

In this equation, Φ is the heating rate, X is the volume fraction crystallized at a specified temperature T, and X is the given ratio of the partial area crystallized at a certain temperature to the total area of the crystallization exotherm. The total area of the crystallization exotherm is between the temperature T_i at which crystallization just begins and the temperature T_f at which the crystallization is complete. The partial area crystallized at a certain temperature is between T_i and T (Cheng et al. 2005). A plot of $\mathrm{Ln}[-\mathrm{Ln}(1 - X)]$ versus $\mathrm{Ln}\Phi$ should
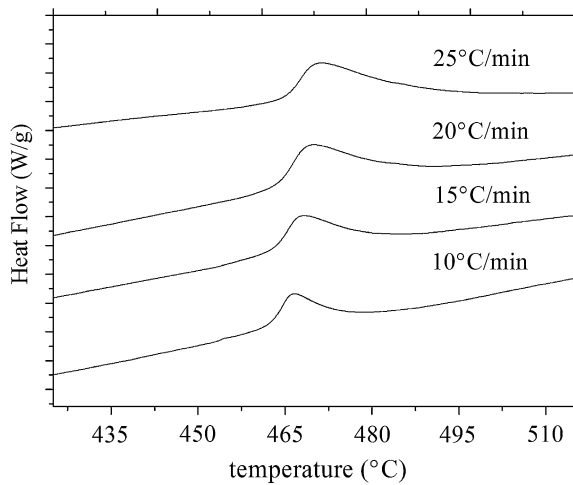
Fig. 6 Differential scanning calorimetry curves of as-synthesized BIT nanocrystals at different heating rates of 10, 15, 20 and 25 °C/min, respectively
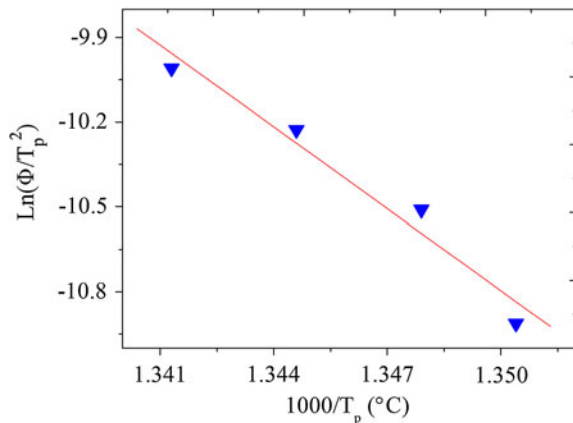

Fig. 7 Plot of $Ln(T_p^2/\Phi)$ versus $1,000/T_p$ for determining the value of crystallization activation energy of as-synthesized BIT nanocrystals

be a straight line. In this equation, n can be calculated from the slope. A value of n close to 3 indicates bulk or three-dimensional crystal growth and a value close to 1 indicates surface growth. Intermediate values of n between 1 and 3 indicate that the surface and internal crystallization occur simultaneously (Francis 2005). The Ozawa plot of $Ln[-Ln(1 - X)]$ versus $Ln\Phi$ is shown in Fig. 8, where the volume fraction crystallized was calculated at a fixed temperature of 467 °C. The value of n is determined from the slope to be 2.25 ± 0.26. This result indicates that the crystallization is dominated by a surface and an internal crystallization process simultaneously.
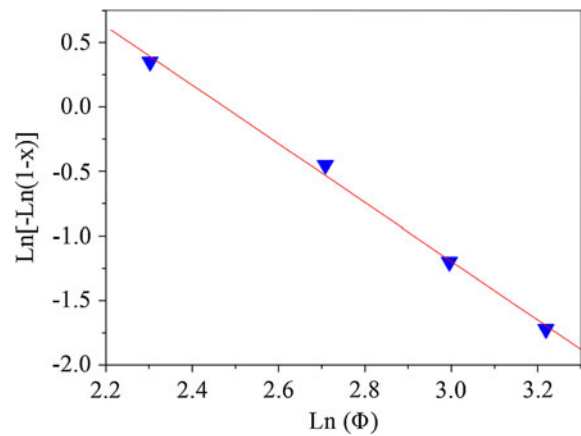
Fig. 8 Plot of $Ln[-Ln(1 - X)]$ versus $Ln\Phi$ for the calculation of Avrami constant, n of BIT nanocrystals

Matusita and Sakka (1979, 1980) proposed that the Kissinger model is only valid when crystal growth occurs on a specified number of nuclei; otherwise, incorrect values for the activation energy are obtained. Therefore, they modified the Kissinger equation to account for nucleation and crystallization growth occurring simultaneously to where E_a is the activation energy of crystallization and m represents the dimensionality of the crystalline phase. n and m correspond to each other through the relation $m = n - 1$. Figure 9 shows the Matusita and Sakka plot for the determination of activation energy of crystallization, where the m value is equal to 1.25. Using $n = 2.25 \pm 0.26$ and $m = 1.25 \pm 0.26$, the
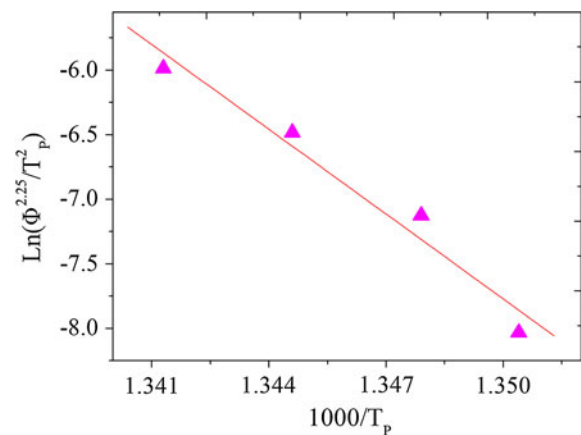
Fig. 9 Plot in accordance with the Matusita and Sakka equation for the determination of the activation energy for crystallization

modified Kissinger plot gave an activation energy of 220.84 ± 2.73 kJ/mol.
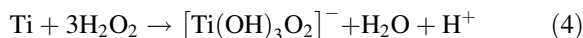
FT-IR analysis

Figure 10 shows FT-IR spectra of the initial precursors at room temperature, and the resulting products after these gels were treated at different temperatures of 450–800 °C. All of these regions represent one or more characteristic bands, referring to the different functional groups that are present in the $Bi_4Ti_3O_{12}$ nanocrystals. The spectra show the decomposition of the peroxo complexes present in the precursors and their rearrangements into the inorganic crystalline phases. The room temperature spectra of the BIT and Ti-peroxy gels are very similar. The peaks in the region of 3,500–3,000 cm^{-1} are assigned to the characteristic stretching vibration of water and the stretching vibrations of hydroxyl groups. Three weak peaks localized at 2399, 1762 and 1612 cm^{-1} for Ti-peroxy gel are from crystal water (Parkyns 1970). The occurrence of several bands at 1,373 cm^{-1} during the Ti-peroxy gel indicates that is released H_2O_2 during Ti-peroxy nanocrystal degradation, which is similar to the report (Tengvall et al. 1991). This conclusion is supported by the FT-IR spectra if we assign the bands at 883 and 825 cm^{-1} to free H_2O_2 or to $Ti–H_2O_2$ (Chin and Giguere 1961). Compared to the Ti-peroxy gel, similar peaks were obtained from BIT gel.

As the heat-treatment temperature for BIT precursors is increased up to 800 °C, the two broad peaks at 350–1,000 cm^{-1} that existed at room temperature evolves into two obvious peaks at 586 and 817 cm^{-1} due to the M–O vibrations, which corresponds to the formation of crystalline BIT. This result is also consistent with the XRD patterns shown in Fig. 1, supporting the fact that pure BIT phase is obtained at 550 °C. The band at 586 and 817 cm^{-1} can be attributed to the stretching vibration of Ti–O and Bi–O bands, which is in agreement with the report (Gu et al. 1998).

Fig. 10 FT-IR spectra of the BIT precursors : **a** Ti-peroxy and BIT gel; **b** *a* 500, *b* 550, *c* 600, *d* 700 and *e* 800 °C for BIT nanocrystals
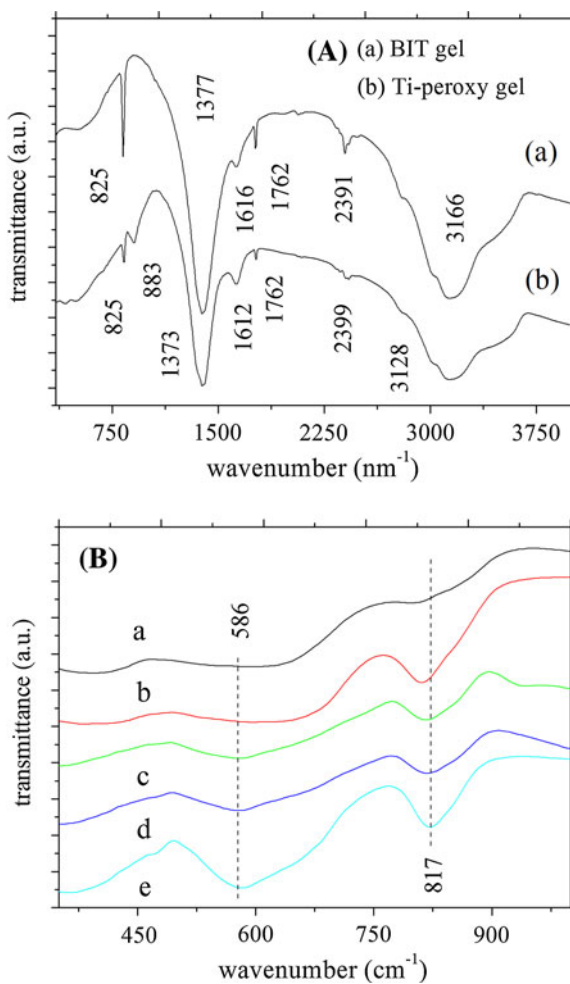
Chemistry mechanism

Aqueous solutions of Ti(IV) and hydrogen peroxide give an intense orange colour in concentrated solutions, characteristic of peroxo complexes, such as peroxytitanato $[Ti(OH)_3O_2]^-$ ion, often referred to as peroxititanic acid. The mechanism responsible for the radical formation was suggested to be bulk trapping of "free oxygen radicals" formed during the $Ti–H_2O_2$ interaction. At high pH, the superoxide (O_2^-) was replaced by hydroxyl ions in the inner coordination sphere of the Ti ion. Thus, the reaction can be described by Eq. 2 (Camargo and Kakihana 2001):

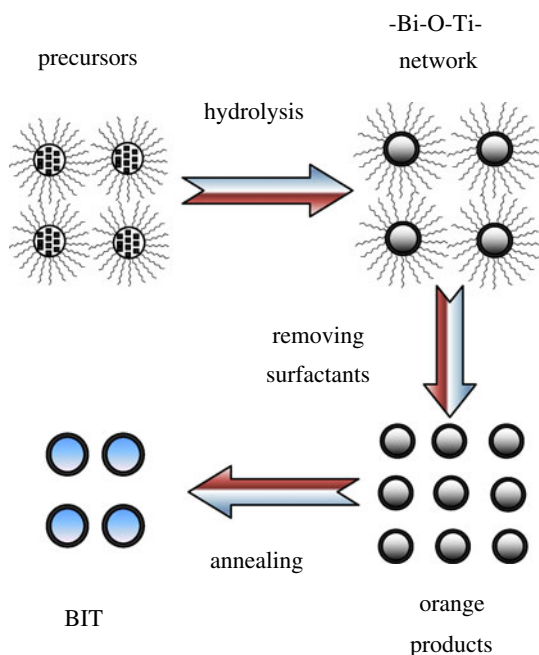$$Ti + 3H_2O_2 \rightarrow \left[Ti(OH)_3O_2\right]^- + H_2O + H^+ \qquad (4)$$

Besides, excess of hydrogen peroxide stabilized the solution of peroxititanic acid, and the soluble bismuth hydroxide formed in the presence of excess of OH^-.

After the precursors containing bismuth and titanium ions were dispersed in the microemulsion including CTAB, *n*-octanol and butanol, the –Bi–O–Ti– network

precursors

-Bi-O-Ti-
network

hydrolysis

removing
surfactants

annealing

BIT

orange
products

Scheme 2 Schematic illustration of the formation process of well-dispersed BIT nanocrystals via the peroxide-based route assisted with the inverse microemulsion process

will be obtained under the benign condition. An orange material after removing surfactants is formed containing these elements at the same precise molar ratio for the peroxititanic acid at high pH value. This precipitate can be described as a mixture of amorphous Bi_2O_3 and TiO_2 at the low temperature, which can be obtained at any desired molar ratio of Bi:Ti. The heat treatment for crystallization and growth leads to nucleation and growth of highly crystalline and monodisperse nanocrystals. Schematic methodology for this facile process is illustrated in Scheme 2. Thus, a significant feature of novel approach is the large-scale quantities of well-dispersed bismuth titanate nanocrystals with higher quantitative yields. Based on this novel route, the material scope can also be extended to related perovskites, such as $(Ba, Sr)TiO_3$ and $PbTiO_3$, greater control over crystal morphology and tunability of dielectric and ferroelectric properties may be realized.

Conclusion

Well-dispersed bismuth titanate nanocrystals were synthesized via the peroxide-based route assisted

with the inverse microemulsion process. A water-soluble peroxititanic complex $[Ti(OH)_3O_2]^-$ was prepared through the reaction between titanium metal and hydrogen peroxide at pH > 7 and a water-in-oil microemulsion, added with a suitable emulsifier, has been used. According to XRD studies, the initial crystallization temperature of bismuth titanate is found to be at 450 °C, whereas that of the fully crystallized BIT appeared at temperatures above 550 °C. The analysis of nonisothermal DSC data yielded a value of 220.84 ± 2.73 KJ/mol and 2.25 ± 0.26 for the activation energy of crystallization (E_a) and the Avrami exponent (n), respectively. TEM patterns showed the well-dispersed BIT nanocrystals with a particle size distribution between 3 and 60 nm after heat-treatment at 550 and 600 °C. All results demonstrate this novel route is a promising way to produce the well-dispersed multi-component perovskite nanocrystals.

References

Aurivillius B (1949) Mixed bismuth oxides with layer lattices. Ark Kemi 1:463–470

Bondurant DW, Gnadinger FP (1989) Ferroelectrics for non-volatile RAMs. IEEE Spectr 26:30–33

Camargo ER, Kakihana M (2001) Peroxide-based route free from halides for the synthesis of lead titanate powder. Chem Mater 13:1181–1184

Cheng CT, Lanagan M, Jones B, Lin JT, Pan MJ (2005) Crystallization kinetic and phase development of PbO–BaO–SrO–Nb₂O₅–B₂O₃–SiO₂-based glass–ceramics. J Am Ceram Soc 88:3037–3042

Chin D, Giguere PA (1961) The torsional oscillation frequency of H₂O₂. J Chem Phys 34:690–691

Damjanovic D (1998) Ferroelectric, dielectric and piezoelectric properties of ferroelectric thin films and ceramics. Rep Prog Phys 61:1267–1324

Francis AA (2005) Non-isothermal crystallization kinetics of a blast furnace slag glass. J Am Ceram Soc 88:1859–1863

Gu HS, Kuang AX, Li XJ (1998) Reactions in preparing Bi₄Ti₃O₁₂ ultrafine powders by sol–gel process. Ferroelectrics 211:271–280

Horn JA, Zhang SC, Selvaraj U, Messing GL, Trolier McKinstry S (1999) Templated grain growth of textured bismuth titanate. J Am Ceram Soc 82:921–926

Hou JG, Qu YF, Ma WB (2007a) Effect of CuO–Bi₂O₃ on low temperature sintered MnZn-ferrite by sol–gel auto-combustion method. J Sol–Gel Sci Technol 44:15–20

Hou JG, Qu YF, Ma WB, Shan D (2007b) Synthesis and pie-zoelectric properties of $(Na_{0.5}Bi_{0.5})_{0.94}Ba_{0.06}TiO_3$ ceramics prepared by sol–gel auto-combustion method. J Mater Sci 42:6787–6791

Hou JG, Kumar RV, Qu YF, Krsmanovic D (2009) Controlled synthesis of photoluminescent $Bi_4Ti_3O_{12}$ nanoparticles from metal-organic polymeric precursor. J Nanopart Res DOI: 10.1007/s11051-009-9624-z

Hou JG, Qu YF, Krsmanovic D, Ducati C, Eder D, Kumar RV (2009) Solution-phase synthesis of single-crystalline $Bi_{12}TiO_{20}$ nanowires with photocatalytic properties. Chem Commun. 3937–3939

Kan YM, Jin XH, Wang PL, Li YX, Cheng YB, Yan DS (2003) Anisotropic grain growth of $Bi_4Ti_3O_{12}$ in molten salt fluxes. Mater Res Bull 38:567–576

Kan YM, Jin XH, Zhang GJ, Wang PL, Cheng YB, Yan DS (2004) Lanthanum modified bismuth titanate prepared by a hydrolysis method. J Mater Chem 14:3566–3570

Kimura T, Yoshimoto T, Iida N, Fujita Y, Yamaguchi T (1989) Mechanism of grain orientation during hot-pressing of bismuth titanate. J Am Ceram Soc 72:85–89

Kissinger HE (1956) Variation of peak temperature with heating rate in different thermal analysis. J Res Natl Bur Stand (US) 57:217–221

Matusita K, Sakka S (1979) Kinetics study of crystallization of glasses by differential scanning calorimeter. Phys Chem Glasses 20:81–84

Matusita K, Sakka S (1980) Kinetics study on crystallization of glass by differential thermal analysis-criterion on application of Kissinger plot. J Non-Cryst Solids 38–39: 741–746

Osamu Y, Noboru M, Ken H (1991) The formation and characterization of alkoxy-derived $Bi_4Ti_3O_{12}$. Br Ceram Trans J 90:111–113

Ozawa T (1971) Kinetic of non-isothermal crystallization. Polymer 12:150–158

Parkyns ND (1970) Chemisorption and catalysis. Hepple Publications, London, p 150

Potdar HS, Ravi V (2004) Synthesis of bismuth titanate by citrate method. Mater Res Bull 39:1993–1998

Stojanović BD, Paiva-Santos CO, Cilense M, Jovalekic C, Lazarević ZŽ (2007) Structure study of $Bi_4Ti_3O_{12}$ produced via mechanochemically assisted synthesis. Mater Res Bull 43:1743–1753

Subbarao EC (1961) Ferroelectricity in $Bi_4Ti_3O_{12}$ and its solid solutions. Phys Rev 122:804–807

Sugibuchi K, Kurogi Y, Endo N (1975) Ferroelectric field-effect memory device using $Bi_4Ti_3O_{12}$ film. J Appl Phys 46:2877–2881

Tengvall P, Wälivaara B, Westerling J, Lundström I (1991) Stable titanium superoxide radicals in aqueous Ti-peroxy gels and Ti-peroxide solutions. J Colloid Interface Sci 143:589–592

Xie LJ, Ma JF, Zhao ZQ, Tian H, Zhou J, Wang YG, Tao JT, Zhu XY (2006) A novel method for the preparation of $Bi_4Ti_3O_{12}$ nanoparticles in w/o microemulsion. Colloids Surf A 280:232–236

Yang QB, Li YX, Yin QR, Wang PL, Cheng YB (2003) $Bi_4Ti_3O_{12}$ nanoparticles prepared by hydrothermal synthesis. J Eur Ceram Soc 23:161–166